Accepted Manuscript

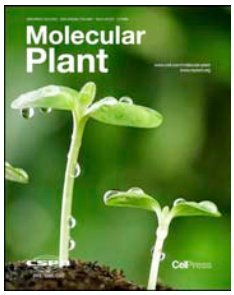

SNARE-RNAi results in higher terpene emission from ectopically expressed caryophyllene synthase in *Nicotiana benthamiana*

Hieng-Ming Ting, Thierry L. Delatte, Pim Kolkman, Johana C. Misas-Villamil, Renier A.L. van der Hoorn, Harro J. Bouwmeester, Alexander R. van der Krol

PII: S1674-2052(15)00093-3

DOI: 10.1016/j.molp.2015.01.006

Reference: MOLP 69

To appear in: *MOLECULAR PLANT*

Received Date: 30 July 2014

Revised Date: 7 January 2015

Accepted Date: 9 January 2015

Please cite this article as: **Ting H.-M., Delatte T.L., Kolkman P., Misas-Villamil J.C., van der Hoorn R.A.L., Bouwmeester H.J., and van der Krol A.R.** (2015). SNARE-RNAi results in higher terpene emission from ectopically expressed caryophyllene synthase in *Nicotiana benthamiana*. Mol. Plant. doi: 10.1016/j.molp.2015.01.006.

Title

SNARE-RNAi results in higher terpene emission from ectopically expressed caryophyllene synthase in *Nicotiana benthamiana*

Hieng-Ming Ting[1], Thierry L. Delatte[1], Pim Kolkman[1], Johana C. Misas-Villamil[2], Renier A.L. van der Hoorn[2,3], Harro J. Bouwmeester[1] and Alexander R. van der Krol[1]

[1]Laboratory of Plant Physiology, Wageningen University, P.O. Box 658, 6700 AR Wageningen, The Netherlands.

[2]Plant Chemetics Laboratory, Max Planck Institute for Plant Breeding Research, Carl-von-Linne Weg 10, 50829 Cologne, Germany

[3]Plant Chemetics laboratory, Department of Plant Sciences, University of Oxford, South Parks Road, Oxford OX1 3RB, United Kingdom.

Author for correspondence: Alexander R. van der Krol;
Tel.: +31317482448 ; Email: sander.vanderkrol@wur.nl

Running title: SNARE-RNAi boosts terpene production

Short summary

We show that coexpression of a *VAMP72-RNAi* (*Vi*) and a caryophyllene synthase (*C*) gene results in higher terpene levels. RNA-sequencing indicates strong interaction upon coexpression of these two genes, resulting in increased levels of ubiquinated proteins. This indicates that reduced protein turnover may contribute to the higher terpene production.

Abstract

Plants produce numerous terpenes and much effort has been dedicated to the identification and characterization of the terpene biosynthetic genes. However, little is known about how terpenes are transported within the cell and from the cell into the apoplast. To investigate a putative role of vesicle fusion in this, we used *Agrobacterium tumefaciens*-mediated transient co-expression in *Nicotiana benthamiana* of an *MtVAMP721e-RNAi* construct (*Vi*) with either a caryophyllene synthase or a linalool synthase, respectively. Headspace analysis of the leaves showed that caryophyllene or linalool emission increased about 5-fold when *N. benthamiana* VAMP72 function was blocked. RNA-sequence and protein ubiquination analysis of the agro-infiltrated *N. benthamiana* leaf extracts suggested that increased terpene emissions may be attributed to proteasome malfunction based on three observations: (1) leaves with *TPS+Vi* showed higher level of a DsRed marker protein, (2) they show higher level of ubiquinated proteins and (3) leaves with *TPS+Vi* show cooordinated induced expression of multiple proteasome genes, presumably caused by lack of proteasome mediated feedback regulation. However, caryophyllene or linalool did not inhibition proteasome related protease activity in *in vitro* assays. While results are not conclusive for a role of vesicle fusion in terpene transport, they do show a strong interaction between inhibition of vesicle fusion and ectopic expression of certain terpenes. Results have potential applications in metabolic engineering.

Keywords: terpene transport, vesicle-associated membrane proteins (VAMP72), caryophyllene synthase, linalool synthase, proteasome, photosynthesis, *Nicotiana benthamiana*.

Introduction

Plants produce numerous volatile terpenoids, which have many different functions, varying from plant hormones to abiotic stress protectants (e.g. heat protection) or in biotic stress responses (e.g. attraction of predators of plant herbivores) (Holopainen and Gershenzon, 2010). Emission of volatile terpenes from plant cells may involve multiple pathways, e.g. (1) insertion of the hydrophobic terpene into vesicle membranes followed by transport and fusion to the plasma membrane, (2) it may involve carrier proteins that transport these molecules to the (plasma) membrane [e.g. similar to the role of GST proteins in flavonoid transport; (Zhao and Dixon, 2010)], (3) membrane ABC transporters may be involved in the translocation of terpenes over the plasma membrane and (4) there could be direct diffusion between the ER and/or plastidial (stromule) membranes and the plasma membrane, possibly through specific contact sites. Multiple transport pathways have also been described for the transport of non-volatile lipids, involving both a vesicle and non-vesicular transport mechanism (Lev, 2010).

As lipophilic compounds would favor sequestering into membranes, one option for transport of terpenes within the cell could be through vesicle transport between subcellular compartments and delivery of the terpenoids to target membranes by vesicle fusion. Hints that terpenoids may be transported by vesicles come from studies on *Plasmodium falciparum* for which it was shown that the sesquiterpene lactone artemisinin is transported from the red blood cell into the parasite (*Plasmodium falciparum*) via parasite-derived membrane vesicles (Eckstein-Ludwig et al., 2003; Gershenzon and Dudareva, 2007). A study on *Sauromatum guttatum* flowers showed fusion of vesicles from the ER with the plasma membrane and this correlated with the heat-induced release of sesquiterpenes (α-copaene and caryophyllene) (Skubatz et al., 1995), hinting at the involvement of vesicle transport and fusion in terpene emission. The results from this study may be an indication that terpenes are stored in vesicles which are transported to the plasma membrane and supposedly fusion of these vesicles with the plasma membrane result in the release of the volatile sesquiterpenes. The fusion of vesicles with target membranes is mediated by a group of proteins called SNAREs (Soluble *N*-ethylmaleimide sensitive factor Attachment protein REceptor) (Lang and Jahn, 2008). One v-SNARE (SNARE protein on the transport vesicle) pairs with three t-SNARE proteins (SNARE proteins on the target membrane, including syntaxins) (Lang and Jahn, 2008), leading to membrane fusion between the two compartments. v-SNAREs consist of long vesicle-associated membrane proteins (VAMPs) or ‘longins’ (containing an N-terminal

longin domain) and short VAMPs or 'brevins' (Filippini et al., 2001). However, in plants only the longin-type v-SNAREs occur, and they can be further classified into three major groups: VAMP7-like, Ykt6-like and Sec22-like (Fujimoto and Ueda, 2012). A sub-group of the VAMP7-likes, the VAMP72 family, has been shown to be involved in exocytosis in plants (Kwon et al., 2008; Sanderfoot, 2007), while a VAMP72 protein from *Medicago truncatula* (MtVAMP721) was shown to be involved in the exocytosis pathway required for arbuscule formation (Ivanov et al., 2012).

Here we addressed the question whether vesicle transport is involved in transport of terpenoids within the cell and whether vesicle fusion plays a role in the emission of the terpenoids into the apoplast. As a model we used the volatile sesquiterpene caryophyllene, which is not easily converted to oxidized and/or glycosylated, non-volatile, compounds upon ectopic production in plants, and the monoterpenoid linalool. To evaluate the role of vesicle transport/fusion we combined transient expression of caryophyllene synthase (*CST*) or linalool synthase (*FaNES*) with a *SNARE-RNAi* construct targeted at *N. benthamiana VAMP72* genes. Surprisingly, the coexpression of *CST* (*C*) with *MtVAMP721e-RNAi* (*Vi*) resulted in 5-fold higher caryophyllene emission levels. Sequence analysis of RNA from samples with *C+Vi* showed a stronger transcriptional response than *C* or *Vi* alone. Specifically a coordinated upregulation of genes encoding components of the 26S proteasome was noted, which may be a hallmark of reduced negative feedback on proteasome gene expression when proteasome functionality is impaired (Kobayashi and Yamamoto, 2005; Villeneuve et al., 2010). Indeed, higher levels of ubiquinated proteins were found in extracts from the *CST+MtVAMP721e-RNAi* agroinfiltrated leaves, indicating that reduced protein turnover may be causal to the higher terpene production. However, caryophyllene did not inhibit protease activity of proteasomes in an *in vitro* assay. Results are discussed in the context of the different pathways that may be involved in terpene emission.

Results

Expression of VAMP72-RNAi enhances transient caryophyllene production

For the production of the volatile sesquiterpene caryophyllene in plants a fragment of *Arabidopsis* genomic DNA was isolated, encoding the caryophyllene synthase (CST) TPS21 and this fragment was fused to the constitutive CaMV35S promoter in a construct we used for transient expression in *N. benthamiana*. Caryophyllene production was assayed by a

headspace trapping assay for isolated leaves, harvested at seven days post agroinfiltration. Pilot studies indicated that substantial amounts of caryophyllene are produced by leaves agroinfiltrated with the *35S:CST* (*C*) construct (data not shown). For the inhibition of *VAMP72* gene expression in *N. benthamiana* we used the *MtVAMP721e-RNAi* (*Vi*) expression construct previously described to inhibit vesicle transport in *Medicago truncatula* (Ivanov et al., 2012). We identified fourteen *VAMP72* genes in *N. benthamiana* and sequence analysis of the *N. benthamiana* genome shows fourteen *VAMP72*-like genes with 67-83% DNA sequence identity to *MtVAMP721e*, with highest DNA sequence identity to *NbVAMP72c* (Figure S1A and S2A). The *MtVAMP721e-RNAi* (*Vi*) was transiently expressed in *N. benthamiana* leaves and RNA was isolated at seven days post agroinfiltration. qRT-PCR analysis using *MtVAMP72c* specific primers indicated that the transient expression of *Vi* reduced *VAMP72c* mRNA levels almost 9-fold compared to the control (Figure S2B), indicating that the heterologous *MtVAMP721e-RNAi* can efficiently target *N. benthamiana VAMP72* genes. Because the high levels of RNAi in transient expression may generate pleiotropic effects on gene silencing (e.g. by titration of Argonaute complexes), we also tested the effect of a *DsRed-RNAi* (*Di*) construct in combination with *35S:CST* (*C*). Note that all vectors containing an RNAi construct also contained a *DsRed* marker gene (see Figure 1).

For all the different treatments the relative dosage of *C* and *Vi* was kept constant by combining expression with *Di*. For *Di* the relative gene dosage was kept constant by combining expression with an empty vector (*pBin*: *P*). To determine the effect on headspace emission of caryophyllene we compared the treatments *pBin+DsRed-RNAi* (*P+Di*), *MtVAMP721e-RNAi+DsRed-RNAi* (*Vi+Di*), *CST+DsRed-RNAi* (*C+Di*) and *CST+MtVAMP721e-RNAi* (*C+Vi*). All treatments were evaluated at seven days post agroinfiltration by harvesting the infiltrated leaves and measuring the amount of caryophyllene that is released into the headspace in 30 minutes in the light. As expected, leaves transiently expressing *P+Di* or *Vi+Di* produced only very low levels of caryophyllene, which can be attributed to endogenous *N. benthamiana* CST activity (Figure 2). However, leaves with *C+Di* produced substantial amounts of caryophyllene in the 30 minutes of headspace trapping (Figure 2). One could expect that if vesicle fusion is involved in caryophyllene transport, inhibition of vesicle fusion by downregulation of *VAMP72* expression would decrease the emission of caryophyllene. However, in the *C+Vi* treated leaves the caryophyllene emission was approximately 5-fold higher (Figure 2). This indicates that inhibition of *N. benthamiana VAMP72* gene expression does affect the flux through the

caryophyllene emission pathway, but in an unexpected way. In total, the experiment was repeated six times, every time yielding similar results. To understand better why the *C+Vi* treatment resulted in higher caryophyllene emission levels we choose to perform RNA-seq on the different leaf samples to investigate the transcriptional response to the different agroinfiltration treatments.

RNA-seq analysis of agroinfiltrated leaves

To better understand how the inhibition of vesicle transport, when combined with *CST*, leads to enhanced caryophyllene emission we performed semi-quantitative sequence analysis on RNA isolated from the agroinfiltrated leaves. For this, RNA was extracted from the leaves at seven days post agroinfiltration of the combinations *P+Di, Vi+Di, C+Di* and *C+Vi* for quantification by RNA-seq (see Materials and Methods). The relative expression levels of genes was compared to that of the control treatment (*P+Di*) and differentially expressed genes between *Vi+Di*, *C+Di* or *C+Vi* and the control were selected, using a threshold of the absolute value of $\log_2$FoldChange $\geq$1 at a false discovery rate (FDR) $\leq$0.05. Figure 3A shows the total transcriptional response of differentially expressed genes and the treatment-specific response (total differential transcriptional response minus the overlap with either of the other two treatments). Results show that inhibition of vesicle fusion (treatment *Vi+Di*) causes upregulation of only 144 and downregulation of 214 genes (Figure 3A). The transcriptional response to caryophyllene overproduction (treatment *C+Di*) was more pronounced, with 619 upregulated and 769 downregulated genes compared to *P+Di*. In contrast, the transcriptional response to the combination of caryophyllene overproduction with inhibition of VAMP72 activity (treatment *C+Vi*) resulted in the upregulation of 1822 genes and downregulation of 1353 genes compared with the control. Also when corrected for the overlap in transcriptional response, the co-expression of *CST* and *MtVAMP721e-RNAi* causes a much larger change in the gene expression profile (1400 up, 1192 down) than the specific response to either *Vi+Di* (49 up, 63 down) or *C+Di* (412 up, 454 down) (Figure 3A). The Venn diagrams of the overlap in transcriptional response for the different treatments are shown in Figure 3B. To get insight in the biological processes affected by the different treatments, a GO-term enrichment analysis was performed on the differentially expressed genes, using $P \leq 0.05$ (Tables S1-S3). In addition, the differentially expressed genes of the different treatments were mapped to the reference canonical plant pathways in the Kyoto Encyclopedia of Genes and Genomes (KEGG) (Tables S4-S6). For each of the three treatments, the top ten of pathways that were most affected are shown in Table S7. The

pathways that were most strongly affected by the different treatments were also visualized via the MapMan tool (Thimm et al., 2004). An overview of all differentially expressed genes between *Vi+Di, C+Di* and *C+Vi* versus control *P+Di* for cellular metabolism is shown in Figure S3. A list of all up- or down-regulated differentially expressed genes corresponding to MapMan functional categories are provided in Table S8.

Transcriptional response to Vi+Di treatment

Analysis of the differentially expressed genes that are specific for *MtVAMP721e-RNAi* shows that the *VAMP72* genes of *N. benthamiana* are most strongly affected (as expected). As a result, the SNARE interaction pathway of vesicular transport shows up for this treatment as the pathway that is strongly affected (Table S7). Figure S1B shows the average number of RNA reads for each member of the *VAMP72* gene family in *N. benthamiana*, for each of the treatments. Results indicate that ten out of the fourteen different *N. benthamiana VAMP72* genes the expression was downregulated in leave samples agroinfiltrated with the *MtVAMP721e-RNAi* construct (*Vi+Di* or *C+Vi*). This indicates that the *M. truncatula MtVAMP721e-RNAi* targets multiple *VAMP72* genes in *N. benthamiana*, but other *VAMP* genes (e.g. *VAMP71* gene family members) are not affected by either the *Vi+Di* or *C+Vi* treatment. Using the threshold of $Q \leq 0.05$, other pathways were not significantly affected by *Vi+Di* (Tables S7). Figure S3A shows the MapMan projection of differentially expressed genes for cellular metabolism, indicating that no major pathway was affected by the *Vi+Di* treatment. Details of the Gene Ontology classification of differentially expressed genes are given in Table S1, S2 and S3. Details of the KEGG enrichment analysis for the *Vi+Di* treatment are given in Table S4.

Transcriptional response to C+Di treatment

Analysis of the transcriptional response to *CST* indicates that ectopic production of caryophyllene is creating a substantial pleiotropic effect in leaves (Table S7). GO term enrichment analysis of the specific differentially expressed genes in the *C+Di* treatment, shows that glucan metabolic processes in cell periphery and cell wall are affected by the ectopic caryophyllene production. In addition, ectopic production of caryophyllene had a strong negative effect on the expression of genes involved in glycosaminoglycan degradation, suggesting a reduced breakdown of glycosaminoglycans. Projection of the data in MapMan shows that *C+Di* also resulted in downregulation of genes involved in cell wall biosynthesis (Figure S3B), while biotic response, heat stress response, calcium signaling and development

232 genes were significantly induced (Table S8). Details of the Gene Ontology classification of
233 differentially expressed genes are given in Table S1, S2 and S3. Details of the KEGG
234 enrichment analysis for the *C+Di* treatment are given in Table S5.
235
236 ***Transcriptional response to the C+Vi treatment***
237 *CST* was a component of the *C+Di* and *C+Vi* treatments, both having the same
238 dosage of the *CST* expression construct in the agroinfiltration. Using the cut-off value
239 $\log_2$FoldChange≥1, the *CST* transgene was not part of the differentially expressed genes.
240 Although the read counts of *CST* in the *C+Di* and *C+Vi* treatments indicated a slightly higher
241 count in the *C+Vi* treatment (1.8-fold) (Figure 4), this is not sufficient to account for the 5-
242 fold increased emission of caryophyllene in this treatment (Figure 2). In the RNA reads we
243 can distinguish between the *Arabidopsis CS*T sequence and *N. benthamiana CST* genes. *N.*
244 *benthamiana* has six genes with close homology to *Arabidopsis CST*. Curiously, the number
245 of RNA reads specific for these endogenous *NbCST* homologs were actually more than two-
246 fold down in *C+Di* and *C+Vi* compared to the *P+D*i treatment (Figure S4).
247 When caryophyllene production was combined with inhibition of VAMP72 function,
248 some of the specific transcriptional responses to *CST* alone were abolished. For instance,
249 compared with the *C+Di* treatment, the *C+Vi* treatment does no longer show a significant
250 increase in differentially expressed genes involved in biotic stress, heat stress and calcium
251 signaling (Table S8). Most interestingly, the combination *C+Vi* specifically upregulates
252 processes related to protein turnover by the 26S proteasome complex and downregulates
253 processes related to photosynthesis (Table S1). Visualization of the output of KEGG for the
254 ubiquitin dependent degradation pathway shows specific upregulation for the *C+Vi* treatment
255 of almost every gene encoding component of the proteasome. These include 14/14
256 components of the proteasome core, 6/9 components of the proteasome lid and 7/9
257 components of the proteaseome base (Figure 5). None of the upregulated genes were affected
258 by the *C+Di* treatment and only one gene was affected by the *Vi+Di* treatment (proteasome
259 lid subunit N6 was down regulated both in *C+Vi* and *Vi+Di* compared to control *P+Di*).
260 Analysis of the data shows that also genes involved in cell wall-related processes
261 were downregulated in the *C+Vi* treatment (Figure S3C). We performed a Wilcoxon rank
262 sum test of differentially expressed genes for the treatments (Table S8) which shows that
263 some genes of the phenylpropanoid pathway (mainly lignin biosynthesis) showed reduced
264 expression (Table S8, Bin 16.2). Besides the many genes involved in cellular processes for
265 which expression was downregulated by the *C+Vi* treatment, a number of transcription

factors were upregulated by this treatment (e.g. AP2/EREBP, C2C2(Zn) CO-like, MADS box transcription factor family) (Table S8, Bins 27.3.3, 27.3.7 and 27.3.24). The upregulation of these transcription factors may explain why so many more genes are affected in the *C+Vi* treatment compared to the other treatments (*Vi+Di*, *C+Di*) in which just few transcription factors were induced (Figure 3, Table S8). Details of the Gene Ontology classification of differentially expressed genes are given in Table S1, S2 and S3. Details of the KEGG enrichment analysis for the *C+Vi* treatment are given in Table S6 and details of the Wilcoxon rank sum test of differentially expressed genes is given in Table S8.

Indications of reduced proteasome activity in the C+Vi treatment

Results from the transcriptional response to *CST+MtVAMP721e-RNAi* (*C+Vi*) indicate a coordinated upregulation of genes encoding the lid, base and core particle of the 26S proteasome complex. From yeast and mammalian studies it is known that transcriptional control of proteasome genes is under feedback regulation by a transcription factor (NF-E2-related factor 2, Nrf2), which itself is targeted for degradation by the 26S proteasome (Kobayashi and Yamamoto, 2005). When proteasome function is impaired, the activity of this transcription factor increases and consequently so does the expression of proteasome genes (Meiners et al., 2003). Although such feedback regulation has not been described for plants yet, the upregulation of proteasome gene expression in response to the *C+Vi* treatment in *N. benthamiana* (Figure 5) could be indicative of reduced proteasome activity. If indeed proteasome function in impaired in the *C+Vi* treatment, this could then also account for the higher caryophyllene emissions if enzymes in the caryophyllene biosynthesis pathway display higher protein stability.

The *DsRed* gene is part of all RNAi constructs, but the treatments *P+Di*, *Vi+Di* and *C+Di* also contain a *DsRed-RNAi* construct. Indeed, in these treatments the expression level of *DsRed* was low, while the number of counts for *DsRed* RNA were high in the *C+Vi* treatment (data not shown).

To get further information on possible effects on protein stability in the *C+Vi* treatments, we analyzed the effect on DsRed protein accumulation. In a separate experiment we tested the effect of an empty *RNAi* vector (*Ei*, which only contains a small linker) on CST activity. Leaves transiently expressing *C+Ei* emitted similar levels of caryophyllene as *C+Di*, while again *C+Vi* stimulated caryophyllene emission (Figure 6A, compare to Figure 2). Because both the *Ei* and *Vi* vector contain the *35S:DsRed* gene, we now could also compare the accumulation of DsRed protein in the combinations *C+Ei* and *C+Vi*. Leaves infiltrated

with *C+Vi* visually had a higher DsRed level than the empty vector control (Figure 6B). Semi-quantification of the signal in the red and green components of the images - setting the average signal for the red (DsRed) and green (chlorophyll) channel of the *C+Ei* image at 100% - showed a significant increase of about 25% for the red signal in the *C+Vi* treatment (Figure 6C), indicating reduced turnover of the DsRed protein in this treatment. In the same leaf the green signal was reduced by 10% (Figure 6C), which is in accordance with the reduction in photosynthesis related gene expression (Figure S3C). Because DsRed protein turnover is supposedly to be mediated by the proteasome (Verkhusha et al., 2003), these results support the interpretation that in the *C+Vi* treated leaves the 26S proteasome activity is reduced.

Protein ubiquination levels are specifically increased in C+Vi agroinfiltrated leaves

Proteins are targeted for degradation by protein ubiquination after which the proteins are recognized by the regulatory particle of the 26S proteasome, which delivers the ubiquinated protein to the proteasome core for protein degradation. If protein degradation is indeed inhibited in leaves expressing *C+Vi*, for instance because of inactivity of the 26S proteasome, this is expected to result in a higher level of ubiquinated proteins. We therefore analyzed protein extracts from the leaves from the different treatments for protein ubiquination levels, using Western blot and a ubiquitin specific antibody. As multiple proteins are targeted for ubiquination and multiple ubiquitins are attached to the same protein, the signals of ubiquinated proteins on a Western blot are not distinct but diffuse, covering many masses. The signal of ubiquinated proteins from extracts with the different treatments was quantified and corrected for small differences in loading of the samples as determined by CBB staining of replicate gels. Results show that indeed the signal in the extracts from leaves with *C+Vi* was 1.8-fold higher than in the extracts from leaves with *C+Di* (Figure 7, for original Western blot see Figure S5). The increased levels of ubiquinated proteins in *C+Vi* agroinfiltrated leaves does suggest that indeed proteasome function in impaired by this combined treatment. Subsequently we tried to investigate what can be the cause of proteasome inhibition in the *C+Vi* treatment.

Caryophyllene does not inhibit 20S proteasome activity in in vitro assays

We tested whether caryophyllene can affect protease activity of the proteasome directly in an *in vitro* assay. The protease activity of the proteasome can be monitored using a fluorescent probe (MVB003) which covalently links to the active sites of the caspase-like

(β1), trypsin-like (β2) and chymotrypsin-like (β5) proteasome catalytic subunits that are part of 20S core particle (Kolodziejek et al., 2011). Thus, fluorescent labeling by MVB003 of these proteases can be used as a measure for proteasome activity in a protein extract. Proteasome fractions were obtained from *N. benthamiana* leaves and incubated with the MVB003 probe combined with increasing amounts of caryophyllene. Results show that the labeling of the protease activity in the proteasome was not affected by caryophyllene up to a concentration of 100 μM in these *in vitro* assays (Figure 8A).

No reduced 20S proteasome activity in extracts from C+Vi agroinfiltrated leaves

While no indications were found that caryophyllene directly affects protease activity of the 20S proteasome, it could be that caryophyllene has an indirect effect on proteasome function, which may require longer time. For instance, part of the caryophyllene in the cell may be converted to caryophyllene oxide and this compound was shown before to cause the formation of reactive oxygen species (Park et al., 2011). Oxidative damage is known to cause disassociation of the 19S and 20S particles, where the 20S proteasome remains functional, and may lead to 19S inactivation by kinase activity (Lee et al., 2010). Therefore we tested whether protein extracts from the leaves agroinfiltrated with either *C+Di, C+Vi, Vi+Di* or *P+Di* showed signs of reduced protease activity. Proteasome containing protein fractions were prepared as described before (see Material and Methods) and the proteasome activity in the extracts was tested with and without additional 100 μM caryophyllene. Results showed that the proteasome activity in leaves with *C+Vi* was not lower than in leaves from any of the other treatments and again, activity was not influenced by the addition of caryophyllene (Figure 8B). We did note a trend of higher labeling of proteasomes in the *C+Vi* fractions, suggesting a higher level of proteasome particles in these samples (Figure 8B). This is in agreement with the higher expression of proteasome related genes in the *C+Vi* leaves (Figure 5), but still raises the question why the level of ubiquinated proteins is elevated in these samples (Figure 7).

General oxidative damage may result in protein carbonylation, and carbonyl moieties allow for derivatization with 2,4-dinitrophenylhydrazine (DNPH), which leads to the formation of a stable dinitrophenylhydrazone (DNP) product. Such modified proteins may be separated PAA gel electrophoresis followed by the identification of the DNP moieties of the protein on Western blots using anti-DNP antibodies and such OxyBlots™ may be used for determination of total protein carbonyl formation (Xiong et al., 2007). However, analysis of

proteins by the OxyBlot procedure did not give any indication of increased oxidative damage in the *C+Vi* treated leaves (Figure S6).

Combined these assays show that neither there are indications of reduced proteasome levels, nor protease activity and no trace of increased oxidative protein damage was found in *C+Vi* treated leaves.

Also other terpene synthases increase protein stability

To test whether inhibition of vesicle fusion by *MtVAMP721e-RNAi* can be used to boost production of other terpenes, we repeated the experiment with a linalool synthase (plastid targeted FaNES, cloned from strawberry). Transient expression of *FaNES* (*F*) in *N. benthamiana* leaves results in the emission of the monoterpenoid linalool into the headspace (Figure 9A). When *FaNES* expression was combined with *MtVAMP721e-RNAi* expression (*F+Vi*) the linalool production was enhanced about 8-fold (Figure 9A), similar to the stimulatory effect of *Vi* on caryophyllene emissions (Figures 2 and 6A). Previously, it was shown that part of the linalool produced in leaves of transgenic plants is converted to glycosylated linalool products (Aharoni et al., 2003; Lücker et al., 2001), but linalool captured in these soluble products can be released by glycosidase treatment. Extracts isolated from leaves agroinfiltrated with *F+Ei* or *F+Vi* were treated with glycosidases and the volatiles released by this treatment were quantified by GC-MS analysis. Results indicated that also the accumulation of glycosylated linalool products was boosted by the *F+Vi* treatment compared with the *F+Ei* treatment (data not shown). The boosting of the linalool production correlated with increased stability of the DsRed marker protein, as the *F+Vi* treatment resulted in more red leaves than the *F+Ei* treatment (Figures 9B and 9C). Combined, the results show that both sesquiterpene and monoterpene can be boosted when VAMP72 mediated vesicle fusion is inhibited. Also for linalool we tested whether the *in vitro* proteasome activity can be inhibited by linalool, but up to a concentration of 100 μM linalool had no effect on protease labeling (Figure S7).

Discussion

Strong interaction between caryophyllene production and inhibition of VAMP72

Although this study started with the question whether vesicles are involved in the transport of volatile terpenes, results were not conclusive about a direct role of vesicles in

terpene transport. Instead we found an unexpected strong interaction between ectopic expression of a terpene synthase (CST or FaNES) and inhibition of *VAMP72* genes through coexpression with *MtVAMP721e-RNAi* (*Vi*), resulting in higher caryophyllene or linalool emission respectively (Figures 2 and 6). Transcript analysis shows that the treatment of *C+Di* or *Vi+Di* resulted in only a limited transcriptional response compared to the control treatment (*P+Di*) (Figure 3A/B) and that the *Vi* is able to suppress multiple *VAMP72* genes in *N. benthamiana* (Figure S1). However, the RNA-seq analysis of the *C+Vi* treatment showed a stronger transcriptional response than that of *C+Di* and *Vi+Di* combined (Figure 3A/B). Most pronounced is the coordinated upregulation of multiple genes related to the proteasome base, core and lid in *C+Vi* (Figure 5). However, the higher expression of the proteasome related genes does not result in a higher protein turnover, but rather coincides with an apparent increase in protein stability (increased DsRed; Figure 6, increased level ubiquinated proteins; Figure 7). An increase in stability of proteins in the caryophyllene biosynthesis pathway may explain the higher emission of caryophyllene in the *C+Vi* compared to the *C+Di* treatment (Figure 2)

Qualitatively, similar results were obtained by combining linalool synthase (*F*) with *Vi*. The *F+Vi* treatment resulted in both increased linalool emission and accumulation of linalool derived glycosides (Figure 9) indicating that indeed overall production is increased. Because also DsRed accumulation is increased in *F+Vi* leaves, this is indicative of a similar effect on protein stability in *F+Vi* as observed for the *C+Vi* treatments.

Feedback regulation of proteasome genes in N. benthamina?

We interpret the coordinated upregulation of the proteasome genes in the *C+Vi* leaves as the result of a proteasome malfunction. Studies in mammals and yeast have shown that proteasome gene expression is under feedback control of transcription factor(s) which are target for proteasome mediated degradation (Kobayashi and Yamamoto, 2005; Villeneuve et al., 2010). As a result, impaired proteasome function causes stabilization of these transcription factors, resulting in an upregulation of proteasome genes in an attempt to maintain the homeostasis in proteasome functionality (Dreger et al., 2010; Meiners et al., 2003). Presumably, proteasome homeostasis in plants is under a similar transcriptional feedback control. The apparent impairment of proteasome function by the *C+Vi* treatment could therefore explain the upregulation of the expression of proteasome-associated genes in our study (Figure 5, Table S8). In yeast the *Ump1* gene is responsible for *de novo* 20S proteasome formation and if there is a coordinated upregulation of proteasome genes, this

gene is most likely also involved (Ramos et al., 1998). Indeed, besides the proteasome lid, base and core component genes, also the closest homolog of *Ump1* in *N. benthamiana* (*NbS00012508g0011.1*) was upregulated 2-fold in the *C+Vi* treated leaves.

The upregulation of the proteasome genes in *C+Vi* leaves seems not to be sufficient to fully restore proteasome functionality as the level of ubiquinated proteins is still elevated in these leaves (Figure 7) and also our marker protein DsRed shows higher levels of accumulation in *C+Vi* (Figure 6). Recently it was shown that in *Arabidopsis* the genes encoding components of the 26S proteasome are under control of the NAC transcription factor ANAC078 (Nguyen et al., 2013; Yabuta et al., 2011). We blasted the sequence of *ANAC078* to the *N. benthamiana* proteome to identify the putative homologs of *ANAC078* in *N. benthamiana*. The two targets with highest homology to *ANAC078* (*NbS00000666g0007* and *NbS00038001g0007*) did not display any differential transcriptional activity in the leaves with *C+Vi* treatment. Therefore, when either of these proteins is indeed involved in proteasome related gene expression in *N. benthamiana*, the effect of the *C+Vi* treatment on upregulation of proteasome gene expression must be mediated by effects on the stability of these ANA078 homologs.

Additional indirect indications of proteasome impairment in C+Vi agroinfiltrated leaves

The transcriptional activity of the endogenous *NbCST* genes were down in *C+Vi* compared to *P+Di* (Figure S4). Moreover, the RNA-seq analysis indicated that the *C+Vi* treatment resulted in downregulation of the expression of multiple genes of the MVA pathway (*HMGS*, *HMGR*, *IDI*) and the MEP pathway (*MCS*, *HDS*, *IDI*) and the first step towards sesquiterpene biosynthesis (*FDS*) (Figure S8). These effects were specific for *C+Vi* as no down regulation of these genes was observed in either *C+Di* or *Vi+Di*. Although the transcriptional activity of *CST* was slightly higher in the *C+Vi* than in the *C+Di* treatment (Figure 4), we assumed that this alone cannot account for the 5-fold increase in caryophyllene emission by leaves agro-infiltrated with *C+Vi*. The higher caryophyllene emissions may therefore be explained by a decreased turnover of enzymes in the caryophyllene biosynthesis pathway. This inferred increased stability of cayophyllene biosynthesis enzymes may relate to the apparent proteasome impairment in the *C+Vi* treatment.

Recently it was reported that the expression of photosynthesis genes is mainly controlled by the transcriptional repressor PIF3, for which protein stability is regulated by ubiquination and proteasome-mediated degradation (Liu et al., 2013). Impaired proteasome activity could result in stabilization of the *N. benthamiana* PIF3 homolog, resulting in

enhanced suppression of photosynthesis genes, as was observed for the *C+Vi* treatment (Figure S3C). The reduced photosynthesis gene includes reduced activity of magnesium-protoporphyrin O-methyltransferase (NbS00045366g0002.1), a key enzyme in protochlorophylide biosynthesis, which may explain the reduced chlorophyll content in *C+Vi* agroinfiltrated leaves (Figure 6C).

Decreased interaction between proteasome lid and core in C+Vi treated leaves?

While there are multiple indirect (Figures 2, 6, 9 and S8) and direct indications (Figures 5, 7 and S5) of a diminished turnover of (ubiquinated) proteins by the proteasome in the *C+Vi* leaves, it is not clear where this apparent inhibition of proteasome function takes place. For instance, the *in vitro* assay of protease activity of isolated proteasome fractions from *C+Vi* did not show indications of impaired protease activity in the *C+Vi* samples (Figure 8). Actually, the results from the *in vitro* proteasome activity assays hints at increased rather than decreased proteasome related protease activity in the *C+Vi* agroinfiltrated leaves (Figure 8). Also, ectopic expression of *CST* without *Vi* did not result in proteasome impairment and also in an *in vitro* assay caryophyllene did not inhibit the protease activity in isolated proteasome fractions (Figure 8). Therefore, there is a seemingly discrepancy between the proteasome activity as measured in the *in vitro* assays and the reduced degradation of ubiquinated proteins *in planta*. These seemingly conflicting results may still be explained when we assume that the delivery of ubiquinated proteins by the regulatory particle (lid) to the proteasome core (20S) of the 26S proteasome is somehow impaired in leaves agroinfiltrated with *C+Vi*.

Concluding remarks

More research will be needed in the future to investigate whether the interaction between proteasome lid and core is the basis for proteasome impairment in the *C+Vi* treatment. Moreover, it needs to be determined whether caryophyllene and linalool have a specific role in this process. Due to the unexpected effects of inhibition of vesicle transport we remain cautious about the role of vesicles in transport of terpenes. Analysis of a direct effect of vesicle fusions on terpene emission will require time-resolved caryophyllene emission measurements, combined with an inducible *VAMP72-RNAi* construct. Although at present the role of vesicles in terpene transport has not been resolved, our study does show for the first time that terpene production may actually be improved by inhibition of vesicle fusion. Moreover, as proteasomes are targets in cancer research (Yang et al., 2006; Schumacher et

al., 2010; Adams, 2004; Almond and Cohen, 2002; Kupperman et al., 2010), our findings may also provide new leads for the role of terpenes in medical research.

Materials and Methods

Vector construction

35S:DsRed-RNAi. The Gateway pK7GWIWG2(II)-*Q10*::*DsRED* binary vector which contain the red fluorescent marker DsRED1 under the constitutive *Arabidopsis Ubiquitin10* promoter was obtained from Dr. Sergey Ivanov (Ivanov et al., 2012). To construct a *DsRed-RNAi* construct, a 223 bp fragment was amplified using the primer pair attB1-DsRed-F/attB2-DsRed-R (Table S9) using the pK7GWIWG2(II)-*Q10*::*DsRED* vector as template. The amplicon was subcloned into the pDONR221 vector (Invitrogen) using the BP clonase II enzyme mix (Invitrogen) to generate an entry vector pDONR221-DsRed. In a subsequent step, the RNAi fragments were cloned into the pK7GWIWG2(II)-*Q10*::*DsRED* vector through LR recombination (Invitrogen). The vector was transferred to *Agrobacterium tumefaciens* AGL-0 by electroporation. *35S:MtVAMP721e-RNAi* and *35S:EV-RNAi*. *MtVAMP721e-RNAi* and *EV-RNAi* which both contain the *DsRed* reporter gene were kindly provided by Dr. Sergey Ivanov and Prof. Ton Bisseling (Ivanov et al., 2012). *35S:CST*. Genomic DNA was extracted from *Arabidopsis thaliana* (L.) Heynh (Col.0) leaves by the cetyltrimethylammonium bromide (CTAB) method (Chen et al., 2008). A 2160-bp genomic DNA fragment containing 6 introns from start codon to stop codon of caryophyllene synthase (At5g23960) was amplified by PCR using the primer pair CST-F/CST-R (Table S9). The primers used introduce NcoI and NotI restriction sites which were used for cloning into ImpactVectorpIV1A_2.1, which contains the CaMV35S promoter and Rbcs1 terminator (http://www.wageningenur.nl/en/show/Productie-van-farmaceutische-en-industriele-eiwitten-door-planten.htm). The resulting pIV1A_2.1/CST was cloned into the PinPlus binary vector using LR recombination (Invitrogen) (van Engelen et al., 1995). The PinPlus construct containing the *35S:CST* was transferred to *Agrobacterium tumefaciens* AGL-0 using electroporation. *35S:FaNES*. The strawberry linalool/nerolidol synthase, *FaNES*, with a synthetic intron (Yang et al., 2008) was cloned into ImpactVectorpIV1A_2.4, which contains a CaMV35S promoter, plastid targeting signal and Rbcs1 terminator (http://www.wageningenur.nl/en/show/Productie-van-farmaceutische-en-industriele-eiwitten-door-planten.htm) (obtained from Jan G. Schaart, Plant Breeding, Wageningen University).

pIV1A_2.4/FaNES was cloned into the PinPlus binary vector using LR recombination (Invitrogen) (van Engelen et al., 1995).

N. benthamiana VAMP72 gene sequence analysis

To identify the *N. benthamiana VAMP72* genes, we used *Arabidopsis VAMP72* genes to BLAST against the *N. benthamiana* genome sequence which resulted in 14 *NbVAMP72* genes. The percentage of sequence similarity between *MtVAMP721e* and *NbVAMP72s* was calculated using BLAST (Altschul et al., 1997) at the NCBI website (http://blast.ncbi.nlm.nih.gov/).

Transient expression assays in N. benthamiana

Transient expression in leaves of *N. benthamiana* was done as previously reported (Ting et al., 2013). The total dosage of *Agrobacterium tumefaciens* within each experiment was kept constant for the different gene combinations. *N. benthamiana* leaves were infiltrated with *Agrobacterium* containing the following expression constructs: (1) *pBin+DsRed-RNAi*, (2) *MtVAMP721e-RNAi+DsRed-RNAi*, (3) *CST+DsRed-RNAi*, (4) *CST+MtVAMP721e-RNAi*, (5) *CST+EV-RNAi*, (6) *FaNES+MtVAMP721e-RNAi*, (7) *FaNES+EV-RNAi* (six plants per construct, one leaf per plant). Infiltrated leaves were harvested seven days post agroinfiltration. Per sample two leaves were pooled, resulting in three biological replicates for each treatment.

Headspace trapping and analysis of volatiles by GC-MS

The volatile headspace of the agro-infiltrated *N. benthamiana* leaves was analysed by placing leaves in a vial with water to prevent dehydration, and placing the vial in a 1 L glass jar from which volatiles were collected for 30 minutes (between 13:45 pm and 14:15 pm) using dynamic headspace trapping as described (Houshyani et al., 2013). The headspace samples were analysed by GC-MS as described (Houshyani et al., 2013). Terpenoids were identified by comparison of mass spectra and retention time with authentic standards: caryophyllene (Sigma-Aldrich) and linalool (Fluka). Quantification of terpene levels was accomplished by determining the peak area of the characteristic *m/z* (133 for caryophyllene and 71 + 93 for linalool).

RNA isolation

After harvest, leaves were immediately frozen in liquid nitrogen and ground to a fine powder for RNA isolation. RNA was extracted using the RNeasy® Plant Mini kit (Qiagen, Hilden, Germany) with on-column RNase-Free DNase digestion (Qiagen, Hilden, Germany). The quantity and quality of RNA for qRT-PCR was determined using a NanoDrop (NanoDrop Technologies, USA) and agarose gel electrophoresis. For RNA-seq analysis the RNA quality was checked using an Agilent 2100 Bioanalyzer (Agilent, Santa Clara, CA, USA).

Quantitative reverse transcription PCR (qRT-PCR)

cDNA was transcribed from 1 µg of RNA using the iScript cDNA Synthesis kit (BioRad, USA) and diluted 20-fold before use as template for qRT-PCR. A gene specific primer pair NbVAMP72c-F/NbVAMP72c-R was used for PCR. GADPH was used for normalization (Torres-Barceló et al., 2008) (Table S9). Each PCR reaction mixture contained 1 µL cDNA template, 2 µL of each primer (3 µM), 10 µL of iQ™ SYBR® Green Supermix master mix (Biorad) and 5 µL of deionized water. The PCR was performed in the iCycler iQ5 system (BioRad) using a three-step temperature program: (1) 95°C for 3 minutes, (2) 40 cycles of 95°C for 10 seconds, 55°C for 30 seconds and (3) 95°C for 1 minutes, followed by melting curve analysis from 65 to 95°C. Relative expression values were calculated using the efficiency δCt (cycle threshold) method (Livak and Schmittgen, 2001).

RNA-sequencing and data analysis

Construction of the cDNA libraries and subsequent Illumina paired-end sequencing (Illumina Hiseq™ 2000) was performed by BGI, China. The processed and raw data are available from the Gene Expression Omnibus (GEO: GSE60061). The processed reads were assembled by BGI, using the available *N. benthamiana* genome sequence as template (Bombarely et al., 2012), which was carried out using the SOAPaligner/SOAP2 program with the default settings (Li et al., 2009). The gene expression level was calculated using the RPKM method (Reads Per kb per Million reads) (Mortazavi et al., 2008). We used a false discovery rate (FDR) ≤ 0.05 and the absolute value of log2Ratio ≥ 1 as the threshold to select significance of gene expression differences. Differentially expressed genes were then used for gene ontology (GO) functional analysis, using Blast2GO (Conesa et al., 2005). For pathway analysis, we mapped all differentially expressed genes to terms in the Kyoto Encyclopedia of Genes and Genomes (KEGG) (Ogata et al., 1999). MapMan was used to visualize gene

expression changes, using the tomato pathways (http://mapman.gabipd.org/web/guest/mapmanstore) (Thimm et al., 2004).

Analysis of proteasome activity

Ubiquinated protein Western blot: 26S protein ubiquination level was inferred from semi-quantified ubiquitinylated protein levels on Western blots. Liquid nitrogen frozen agroinfiltrated leaf material was fractured with two (5/35) metal bullets by a dismembrator at 30 sweeps/s. Proteins were extracted in a fresh 50 mM Tris-Hcl (pH8; Biomol GmbH, Hamburg, Germany) buffer of 4°C with 5 mM dithiothreitol (DTT), 2 mM sodium dodecyl sulfate (SDS; Fisher Scientific, Massachusetts, USA) and a complete protease inhibitor cocktail tablet (cOmplete that also delivers 1mM EDTA; Roche Diagnostics Nederland B.V., Flevoland, the Netherlands) [adapted from (Lough et al., 1998)]. Samples were prepared for SDS-Polyacryl amide gel electrophoresis (SDS-PAGE) through a 4% stacking gel and 7.5% running gel (from 30% acrylamide/bis; 37.5:1; Bio-Rad Laboratories, California, USA). Gels were stained with Coomassie Brilliant Blue (CBB) [according to (Wondrak, 2001)] to judge the loading equality or were blotted onto a 0.45 µM pore Polyvinylidene difluoride (PVDF) membrane (Thermo Scientific, Illinois, USA) at 4°C under a constant voltage (90V; 20mA/blot) for 60 minutes. Excess protein was discarded from the blot with Tris-buffered saline (TBS). Blocking buffer [TBS with 5% non-fat dried milk (FrieslandCampina, Utrecht, the Netherlands)] was applied to the blot for 60 minutes at room temperature. Ubiquitinylated proteins were targeted by polyclonal anti-UBQ11 rabbit antibodies (antibodies-online.com, GmbH, Aachen, Germany). Repeated washing with TBS, incubation with secondary anti-rabbit antibodies from goat (GE Healthcare UK Limited, Buckinghamshire, UK) and further washing prepared the incubation with luminol (GE Healthcare UK Limited, Buckinghamshire, UK). Luminol oxidation and excitation was catalyzed by horse radish peroxidase ligated to the secondary antibodies for one minute. An Acton Pixis 1024 camera (Princeton Instruments, New Jersey, USA), air-cooled to -78°C, recorded the ubiquitin derived luminescence for 20 seconds of exposure time. Gray scale CBB and luminescence signals were semi-quantified with the Measure Mean gray value function of the software program ImageJ.

Protein oxidation Western blot: As a source of 26S proteasome disintegration, oxidative damage to proteins was probed. Using the OxyBlot™ kit (Merck KGaA, Hesse, Germany)

protein carbonylation was visualized on a Western blot. Carbonyls were derivatized with 2,4-dinitrophenylhydrazine (DNPH) in extension to the protein extraction. To this end, 5% SDS was dissolved in the protein extract prior to an equal volume of a low pH buffer with 2,4-dinitrophenylhydrazine (according to the instruction manual). With the addition of neutralization buffer after 15 minutes the reaction to 2,4-dinitrophyenylhydrazone (DNP) was discontinued. A 100x dilution of rabbit primary anti-DNP antibodies (OxyBlot, Merck KGaA, Hesse, Germany) in blocking buffer was applied to the Western blot that was prepared, processed and examined as described for the ubiquinated protein Western blot.

Proteasome activity measurements: Four leaves of each sample (approx. 2.5 gr of tissue) were ground in 5 mL buffer containing 2 mM DTT and 67 mM Tris pH 7.5. Extracts were centrifuged and filtered through a 0,22 μm PVDF membrane until a clear sample was produced. Protein samples were labeled at room temperature with 1 μM MVB003 for 2 hours in a total volume of 60 μL (Kolodziejek et al., 2011). For the competition assay samples were pre-incubated with different concentrations of caryophyllene (Sigma-Aldrich) or linalool (Fluka) for 30 minutes followed by labeling with MVB003 for 2 hours. An equal amount of all samples were combined and 0.5 – 1% DMSO was added to generate the no-probe-control (NPC). Reaction was stopped by boiling the samples in 1X gel loading buffer (GLB) containing SDS. Protein samples were separated on 12% SDS-PAGE protein gels and fluorescently labeled proteins were detected by in-gel fluorescence scanning using the Typhoon FLA9000 with the following settings: 532 nm laser, BPG1 filter and 1000 PTM sensitivity.

Acknowledgments

H-M.T. was funded by the graduate school of Experimental Plant Sciences (EPS). We also thank the Max Planck Society for financial support. We thank Dr. Sergey Ivanov and Prof. Ton Bisseling for providing *35S:MtVAMP721e-RNAi* and *35S:EV-RNAi* constructs. We thank Jan G. Schaart for providing the pIV1A_2.4/FaNES construct. We would like to thank Francel W.A. Verstappen, Iris Kappers, Geert Stoopen, Roland Mumm, Berhane Weldegergis and Peter Tóth for their assistance with headspace trapping and GC-MS analysis. We thank Desalegn Woldes Etalo for help with MS data analysis, Esmer Jongedijk

for help with the terpene biosynthesis pathway figure, Ralph Bours for help with ImageJ software and Giovanni Melandri who shared the OxyBlot™ kit with us.

Figure legends

Figure 1. Maps of constructs used in this study.

pNOS, promoter of Nopaline Synthase gene; *pAtUbq10*, *Arabidopsis Ubiqutin10* promoter; *p35S*, CaMV35S promoter; *T-nos*, terminator of Nopaline Synthase gene, Kan^R, Kanamycin resistance; Cm^R, Chloramphenicol resistance; *att*R1-*att*R2, recombination sites for LR reaction; *ccdB*, negative bacterial selection marker.

Figure 2. Caryophyllene emission from *Nicotiana benthamiana* leaves.

(A) GC-MS chromatograms showing the caryophyllene emitted from *N. benthamiana* transiently expressing *pBin+DsRed-RNAi* (*P+Di*), *MtVAMP721e-RNAi+DsRed-RNAi* (*Vi+Di*), *CST+DsRed-RNAi* (*C+Di*) and *CST+MtVAMP721e-RNAi* (*C+Vi*). *: caryophyllene.

(B) Mass spectrum of caryophyllene emitted by *N. benthamiana*.

(C) Mass spectrum of caryophyllene standard.

(D) Peak area of caryophyllene produced by leaves of *N. benthamiana*, as detected by headspace GC-MS analysis. Each bar represents the mean of three biological replicates ± SE. Statistically significant different between control (*P+Di*) and treatments (*Vi+Di*, *C+Di* and *C+Vi*) are indicated by an asterisk (Student's *t*-test; ** $p < 0.01$; *** $p < 0.001$).

Figure 3. Overview of transcriptional response relative to the *pBin+DsRed-RNAi* (*P+Di*) treatment.

(A) Total (black) and treatment specific (gray) gene response relative to *P+Di*.

Treatment specific response = total response minus overlap with either of the other treatments.

(B) Venn diagrams showing common genes significantly up- and down-regulated in *N. benthamiana* leaves transiently expressing *Vi+Di*, *C+Di* or *C+Vi* compared to leaves infiltrated with *P+Di*.

(cut-off $\log_2$FoldChange ≥1 and false discovery rate ≤0.05)

V+Di, *MtVAMP721e-RNAi+DsRed-RNA*i; *C+Di*, *CST+DsRed-RNAi*; *C+Vi*, *CST+MtVAMP721e-RNAi*.

Figure 4. Total number of *CST* reads in leaves agroinfiltrated with *pBin+DsRed-RNAi, MtVAMP721e-RNAi+DsRed-RNAi, CST+DsRed-RNAi* and *CST+MtVAMP721e-RNAi.*

All RNAseq data were based on three independent replicates. Error bars indicate standard deviation. Statistically significant different between control (*pBin+DsRed-RNAi*) and treatments (*MtVAMP721e-RNAi+DsRed-RNAi, CST+DsRed-RNAi* and *CST+MtVAMP721e-RNAi*) are indicated by an asterisk (Student's *t*-test; *** $p < 0.001$).

Figure 5. Proteasome genes in leaves agroinfiltrated with *CST+MtVAMP721e-RNAi* that were differentially expressed were mapped in KEEG pathway.

The green and red boxes indicate up or downregulation a gene or a group of genes that is mapped to that category. Whereas, boxes with half green and half red boxes indicate the presence of genes that showed down or upregulation and mapped to the category of gene in the map.

Figure 6. Caryophyllene emission and DsRed stabilization in *CST+MtVAMP721e-RNAi* agroinfiltrated leaves.

(A) Caryophyllene emission in leaves agroinfiltrated with *CST+EV-RNAi* and *CST+MtVAMP721e-RNAi*.

(B) Coloration of leaves seven days post agroinfiltration with *CST+EV-RNAi* and *CST+MtVAMP721e-RNAi*.

(C) Quantification of relative Red and relative Green signal intensities in (B).

Each bar represents the mean of three biological replicates ± SE. Statistically significant different between *CST+EV-RNAi* and *CST+MtVAMP721e-RNAi* are indicated by an asterisk (Student's *t*-test; ** $p < 0.01$; *** $p < 0.001$).

Figure 7. Protein ubiquination levels in agroinfiltrated leaves.

Quantification of ubiquinated protein levels in extracts from *N. benthamiana* leaves transiently expressing *pBin+DsRed-RNAi, MtVAMP721e-RNAi+DsRed-RNAi, CST+DsRed-RNAi* and *CST+MtVAMP721e-RNAi*. Each bar represents the mean of three biological replicates plus Standard Error. Statistically significant different between control (*pBin+DsRed-RNAi*) and treatments (*MtVAMP721e-RNAi+DsRed-RNAi, CST+DsRed-RNAi* and *CST+MtVAMP721e-RNAi*) are indicated by an asterisk (Student's *t*-test; *** $p < 0.001$). For original blot see Figure S5.

Figure 8. Proteasome activity assays.

(A) Proteasome activity is not inhibited by caryophyllene: Fluorescence of proteasome associated protease activity by MVB003 fluorescent labeling in *N. benthamiana* leaf extracts with increasing amount of caryophyllene (0-100 µM).

Bottom: CBB staining of the gel showing sample loading.

(B) Proteasome activity is not lower in *C+Vi* agroinfiltrated leaves: Protein was isolated from *N. benthamiana* leaves agroinfiltrated with *pBin+DsRed-RNAi* (*P+Di*), *MtVAMP721e-RNAi+DsRed-RNAi* (*Vi+Di*), *CST+DsRed-RNAi* (*C+Di*) and *CST+ MtVAMP721e-RNAi* (*C+Vi*) and proteasome related protease activity was visualized using the MVB003 fluorescent labeling, with (+) or without (-)100 µM caryophyllene.

Bottom: CBB staining of the gel showing sample loading.

Figure 9. Linalool emission and DsRed protein stability in *FaNES+MtVAMP721e-RNAi* agroinfiltrated leaves.

(A) Linalool emission in leaves agroinfiltrated with *FaNES+EV-RNAi* and *FaNES+MtVAMP721e-RNAi*.

(B) Coloration of leaves seven days post agroinfiltration with *FaNES+EV-RNAi* and *FaNES+MtVAMP721e-RNAi*.

(C) Quantification of relative Red and relative Green signal intensities in (B).

Each bar represents the mean of three biological replicates ± SE. Statistically significant different between *FaNES+EV-RNAi* and *FaNES+MtVAMP721e-RNAi* are indicated by an asterisk (Student's *t*-test; * $p < 0.05$; *** $p < 0.001$).

References

Adams, J. (2004). The development of proteasome inhibitors as anticancer drugs. Cancer Cell. 5, 417-421.

Aharoni, A., et al. (2003). Terpenoid metabolism in wild-type and transgenic Arabidopsis plants. Plant Cell. 15, 2866-2884.

Almond, J., and Cohen, G. (2002). The proteasome: a novel target for cancer chemotherapy. Leukemia. 16, 433-443.

Altschul, S.F., et al. (1997). Gapped BLAST and PSI-BLAST: a new generation of protein database search programs. Nucleic Acids Res. 25, 3389-3402.

Bombarely, A., Rosli, H.G., Vrebalov, J., Moffett, P., Mueller, L.A., and Martin, G.B. (2012). A draft genome sequence of *Nicotiana benthamiana* to enhance molecular plant-microbe biology research. Mol. Plant Microbe Interact. 25, 1523-1530.

768 Chen, H.J., Wen, I.C., Huang, G.J., Hou, W.C., and Lin, Y.H. (2008). Expression of sweet
769 potato asparaginyl endopeptidase caused altered phenotypic characteristics in
770 transgenic Arabidopsis. Bot. Stud. 49, 109-117.
771 Conesa, A., Gotz, S., Garcia-Gomez, J.M., Terol, J., Talon, M., and Robles, M. (2005).
772 Blast2GO: a universal tool for annotation, visualization and analysis in functional
773 genomics research. Bioinformatics. 21, 3674-3676.
774 Dreger, H., et al. (2010). Protection of vascular cells from oxidative stress by proteasome
775 inhibition depends on Nrf2. Cardiovasc. Res. 85, 395-403.
776 Eckstein-Ludwig, U., et al. (2003). Artemisinins target the SERCA of *Plasmodium*
777 *falciparum*. Nature. 424, 957-961.
778 Filippini, F., Rossi, V., Galli, T., Budillon, A., D'Urso, M., and D'Esposito, M. (2001).
779 Longins: a new evolutionary conserved VAMP family sharing a novel SNARE
780 domain. Trends Biochem. Sci. 26, 407-409.
781 Fujimoto, M., and Ueda, T. (2012). Conserved and plant-unique mechanisms regulating plant
782 post-Golgi traffic. Front Plant Sci. 3, 197.
783 Gershenzon, J., and Dudareva, N. (2007). The function of terpene natural products in the
784 natural world. Nat. Chem. Biol. 3, 408-414.
785 Holopainen, J.K., and Gershenzon, J. (2010). Multiple stress factors and the emission of plant
786 VOCs. Trends Plant Sci. 15, 176-184.
787 Houshyani, B., Assareh, M., Busquets, A., Ferrer, A., Bouwmeester, H.J., and Kappers, I.F.
788 (2013). Three-step pathway engineering results in more incidence rate and higher
789 emission of nerolidol and improved attraction of *Diadegma semiclausum*. Metab. Eng.
790 15, 88-97.
791 Ivanov, S., et al. (2012). Rhizobium-legume symbiosis shares an exocytotic pathway required
792 for arbuscule formation. Proc. Natl Acad. Sci. USA. 109, 8316-8321.
793 Kobayashi, M., and Yamamoto, M. (2005). Molecular mechanisms activating the Nrf2-
794 Keap1 pathway of antioxidant gene regulation. Antioxid. Redox Signal. 7, 385-394.
795 Kolodziejek, I., et al. (2011). Proteasome activity imaging and profiling characterizes
796 bacterial effector syringolin A. Plant Physiol. 155, 477-489.
797 Kupperman, E., et al. (2010). Evaluation of the proteasome inhibitor MLN9708 in preclinical
798 models of human cancer. Cancer Res. 70, 1970-1980.
799 Kwon, C., Bednarek, P., and Schulze-Lefert, P. (2008). Secretory pathways in plant immune
800 responses. Plant Physiol. 147, 1575-1583.
801 Lang, T., and Jahn, R. (2008). Core proteins of the secretory machinery. Handb. Exp.
802 Pharmacol. 184, 107-127.
803 Lee, S.H., Park, Y., Yoon, S.K., and Yoon, J.B. (2010). Osmotic stress inhibits proteasome
804 by p38 MAPK-dependent phosphorylation. J. Biol. Chem. 285, 41280-41289.
805 Lev, S. (2010). Non-vesicular lipid transport by lipid-transfer proteins and beyond. Nat. Rev.
806 Mol. Cell Biol. 11, 739-750.
807 Li, R., et al. (2009). SOAP2: an improved ultrafast tool for short read alignment.
808 Bioinformatics. 25, 1966-1967.
809 Liu, Q., et al. (2011). Reconstitution of the costunolide biosynthetic pathway in yeast and
810 *Nicotiana benthamiana*. PLoS ONE. 6, e23255.
811 Liu, X., et al. (2013). PHYTOCHROME INTERACTING FACTOR3 associates with the
812 histone deacetylase HDA15 in repression of chlorophyll biosynthesis and
813 photosynthesis in etiolated Arabidopsis seedlings. Plant Cell. 25, 1258-1273.
814 Livak, K., and Schmittgen, T. (2001). Analysis of relative gene expression data using real-
815 time quantitative PCR and the 2 (-Delta Delta C (T)) method. Methods. 25, 402-408.
816 Lough, T.J., Balmori, E., Beck, D.L., and Forster, R.L. (1998). Western analysis of
817 transgenic plants. In: Plant Virology Protocols, Springer. 447-451.

Lücker, J., Bouwmeester, H.J., Schwab, W., Blaas, J., Van Der Plas, L.H.W., and Verhoeven, H.A. (2001). Expression of Clarkia S linalool synthase in transgenic petunia plants results in the accumulation of S linalyl d glucopyranoside. Plant J. 27, 315-324.

Meiners, S., et al. (2003). Inhibition of proteasome activity induces concerted expression of proteasome genes and *de novo* formation of mammalian proteasomes. J. Biol. Chem. 278, 21517-21525.

Mortazavi, A., Williams, B.A., McCue, K., Schaeffer, L., and Wold, B. (2008). Mapping and quantifying mammalian transcriptomes by RNA-Seq. Nat. Methods 5, 621-628.

Nguyen, H.M., et al. (2013). An upstream regulator of the 26S proteasome modulates organ size in Arabidopsis thaliana. Plant J. 74, 25-36.

Ogata, H., Goto, S., Sato, K., Fujibuchi, W., Bono, H., and Kanehisa, M. (1999). KEGG: Kyoto Encyclopedia of Genes and Genomes. Nucleic Acids Res. 27, 29-34.

Park, K.R., et al. (2011). β-Caryophyllene oxide inhibits growth and induces apoptosis through the suppression of PI3K/AKT/mTOR/S6K1 pathways and ROS-mediated MAPKs activation. Cancer Lett. 312, 178-188.

Ramos, P.C., Höckendorff, J., Johnson, E.S., Varshavsky, A., and Dohmen, R.J. (1998). Ump1p is required for proper maturation of the 20S proteasome and becomes its substrate upon completion of the assembly. Cell. 92, 489-499.

Sanderfoot, A. (2007). Increases in the number of SNARE genes parallels the rise of multicellularity among the green plants. Plant Physiol. 144, 6-17.

Schumacher, M., et al. (2010). Heteronemin, a spongean sesterterpene, inhibits TNF alpha-induced NF-kappa B activation through proteasome inhibition and induces apoptotic cell death. Biochem. Pharmacol. 79, 610-622.

Skubatz, H., Kunkel, D.D., Patt, J.M., Howald, W.N., Hartman, T.G., and Meeuse, B. (1995). Pathway of terpene excretion by the appendix of *Sauromatum guttatum.* Proc. Natl Acad. Sci. USA. 92, 10084-10088.

Thimm, O., et al. (2004). MAPMAN: a user-driven tool to display genomics data sets onto diagrams of metabolic pathways and other biological processes. Plant J. 37, 914-939.

Ting, H.M., et al. (2013). The metabolite chemotype of *Nicotiana benthamiana* transiently expressing artemisinin biosynthetic pathway genes is a function of *CYP71AV1* type and relative gene dosage. New Phytol. 199, 352-366.

Torres-Barceló, C., Martín, S., Daròs, J.A., and Elena, S.F. (2008). From hypo- to hypersuppression: effect of amino acid substitutions on the RNA-silencing suppressor activity of the *Tobacco etch potyvirus* HC-Pro. Genetics. 180, 1039-1049.

van Engelen, F.A., Molthoff, J.W., Conner, A.J., Nap, J.P., Pereira, A., and Stiekema, W.J. (1995). pBINPLUS: an improved plant transformation vector based on pBIN19. Transgenic Res. 4, 288-290.

Verkhusha, V.V., et al. (2003). High stability of *Discosoma* DsRed as compared to *Aequorea* EGFP. Biochemistry. 42, 7879-7884.

Villeneuve, N.F., Lau, A., and Zhang, D.D. (2010). Regulation of the Nrf2-Keap1 antioxidant response by the ubiquitin proteasome system: an insight into cullin-ring ubiquitin ligases. Antioxid. Redox Signal. 13, 1699-1712.

Wondrak, E.M. (2001). Process for fast visualization of protein. US6319720 B1. LLP, P.W., USA.

Xiong, Y., Contento, A.L., Nguyen, P.Q., and Bassham, D.C. (2007). Degradation of oxidized proteins by autophagy during oxidative stress in Arabidopsis. Plant Physiol. 143, 291-299.

Yabuta, Y., et al. (2011). Involvement of *Arabidopsis* NAC transcription factor in the regulation of 20S and 26S proteasomes. Plant Sci. 181, 421-427.

867 Yang, H., Chen, D., Cui, Q.C., Yuan, X., and Dou, Q.P. (2006). Celastrol, a triterpene
868 extracted from the Chinese "Thunder of God Vine," is a potent proteasome inhibitor
869 and suppresses human prostate cancer growth in nude mice. Cancer Res. 66, 4758-
870 4765.
871 Yang, L.-m., Mercke, P., van Loon, J.J., Fang, Z.-y., Dicke, M., and Jongsma, M.A. (2008).
872 Expression in *Arabidopsis* of a strawberry linalool synthase gene under the control of
873 the inducible potato PI2 promoter. Agr. Sci. China. 7, 521-534.
874 Zhao, J., and Dixon, R.A. (2010). The ‘ins’ and ‘outs’ of flavonoid transport. Trends Plant
875 Sci. 15, 72-80.

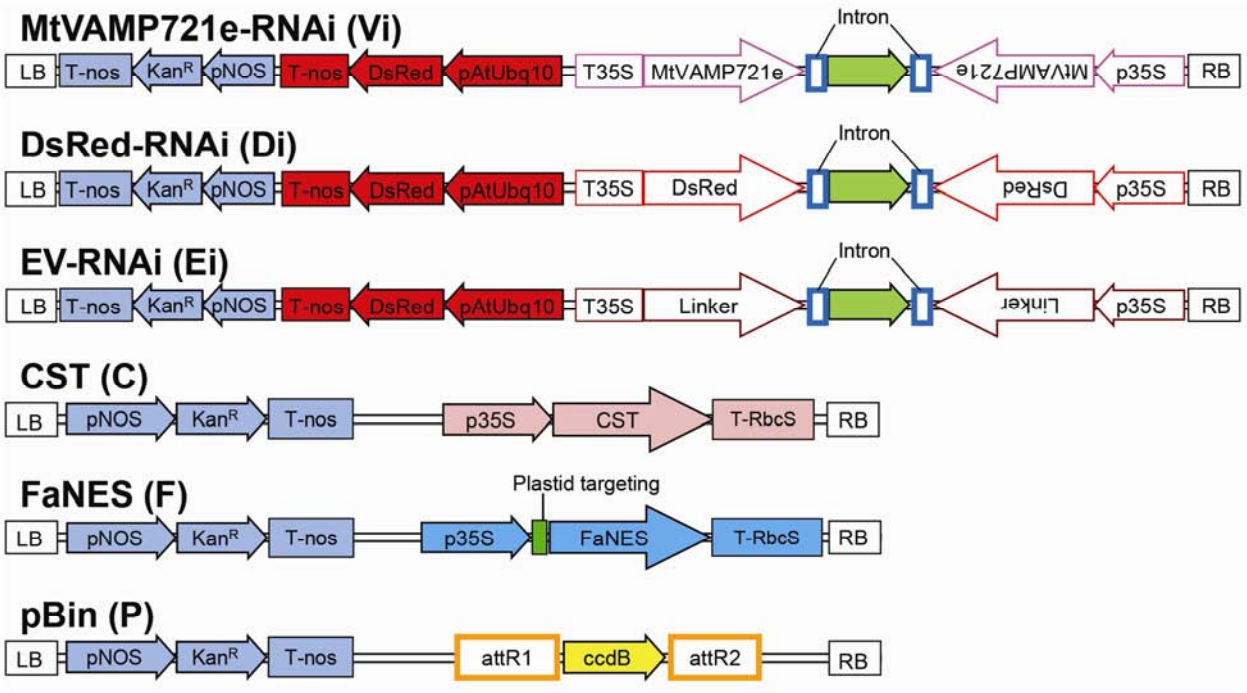

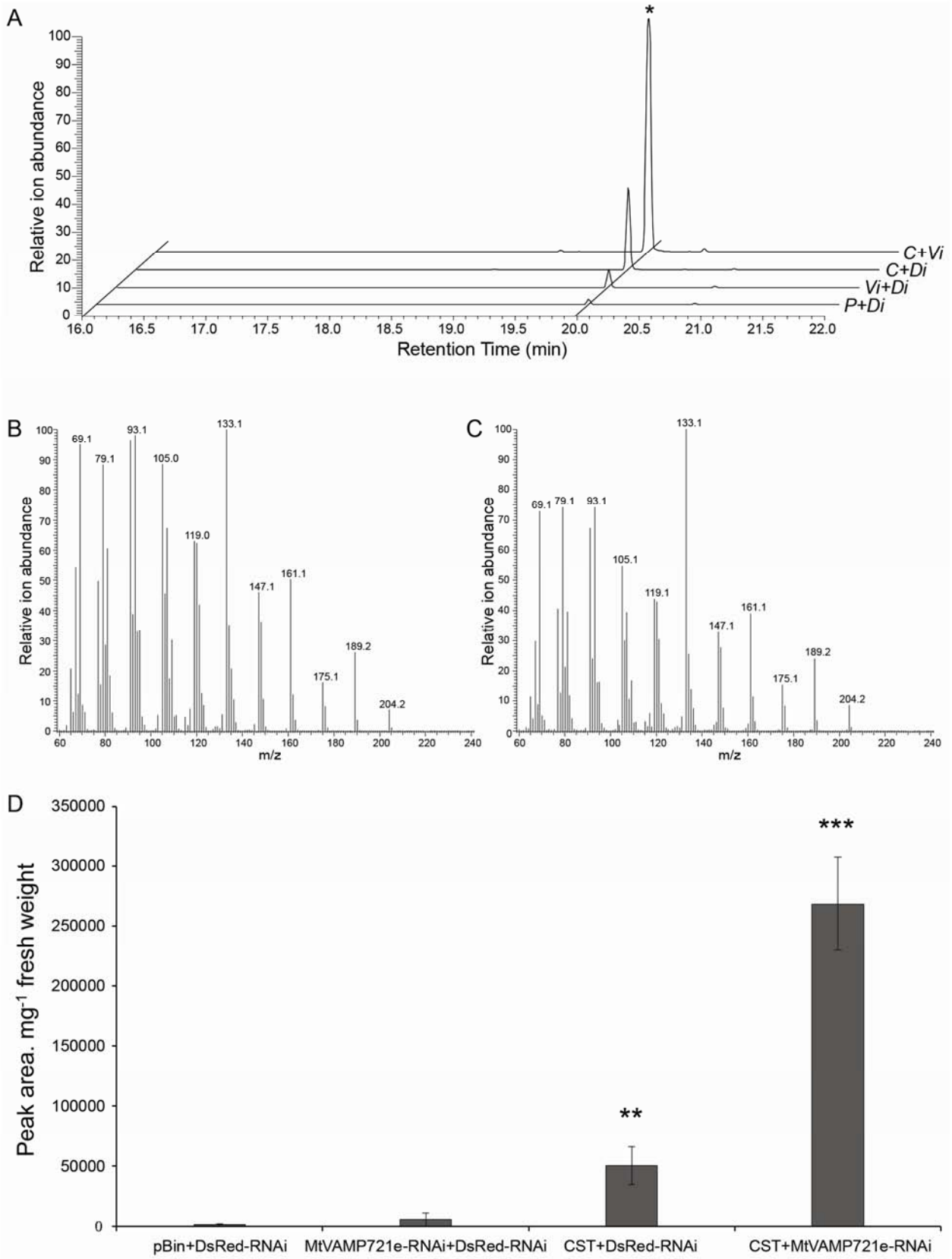
A
Relative ion abundance
Retention Time (min)
*
C+Vi
C+Di
Vi+Di
P+Di
B
Relative ion abundance
m/z
69.1
79.1
93.1
105.0
119.0
133.1
147.1
161.1
175.1
189.2
204.2
C
Relative ion abundance
m/z
69.1
79.1
93.1
105.1
119.1
133.1
147.1
161.1
175.1
189.2
204.2
D
Peak area. mg-1 fresh weight
**
***
pBin+DsRed-RNAi
MtVAMP721e-RNAi+DsRed-RNAi
CST+DsRed-RNAi
CST+MtVAMP721e-RNAi

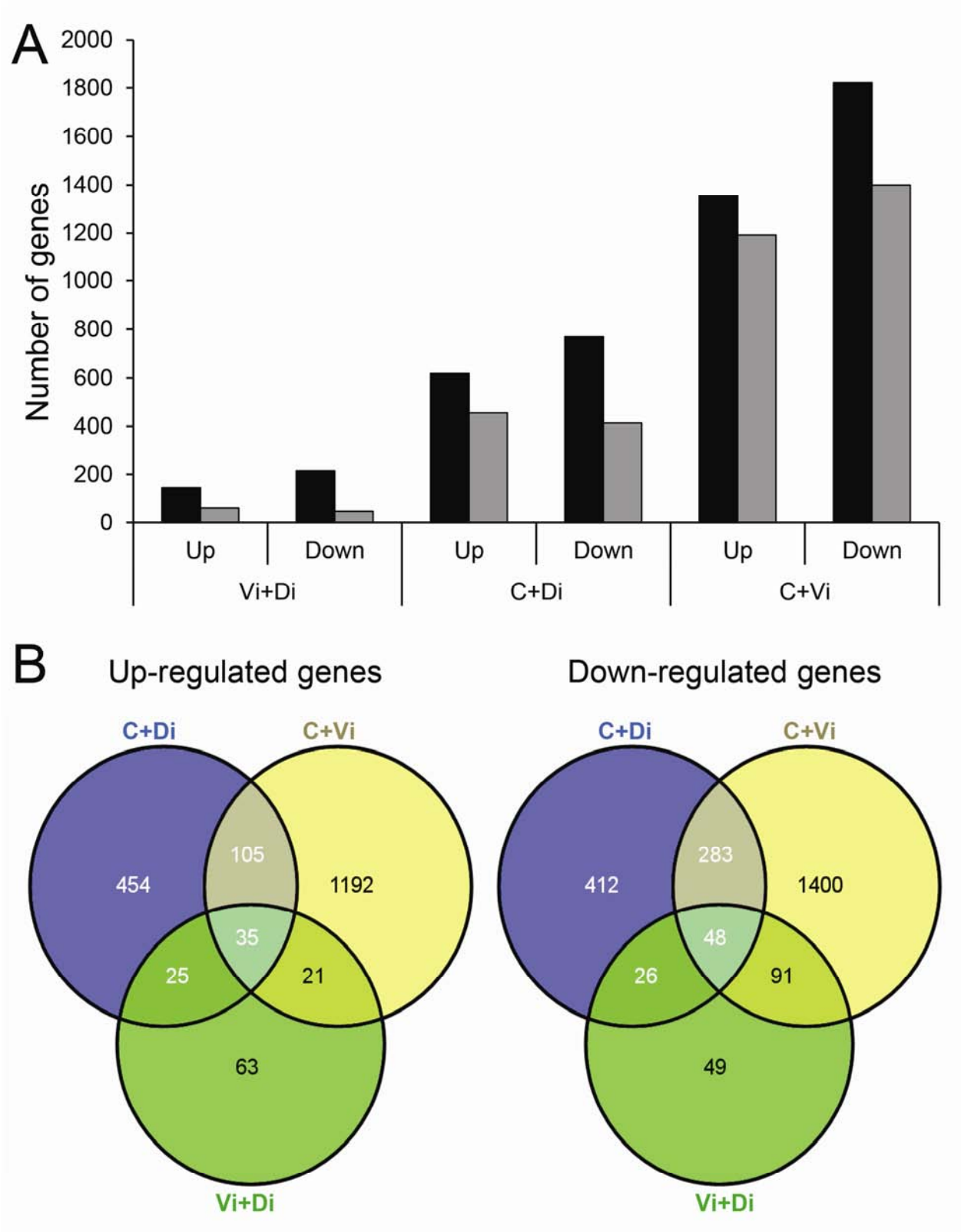
A
Number of genes
2000
1800
1600
1400
1200
1000
800
600
400
200
0
Up
Down
Up
Down
Up
Down
Vi+Di
C+Di
C+Vi
B
Up-regulated genes
Down-regulated genes
C+Di
C+Vi
454
105
1192
35
25
21
63
Vi+Di
C+Di
C+Vi
412
283
1400
48
26
91
49
Vi+Di

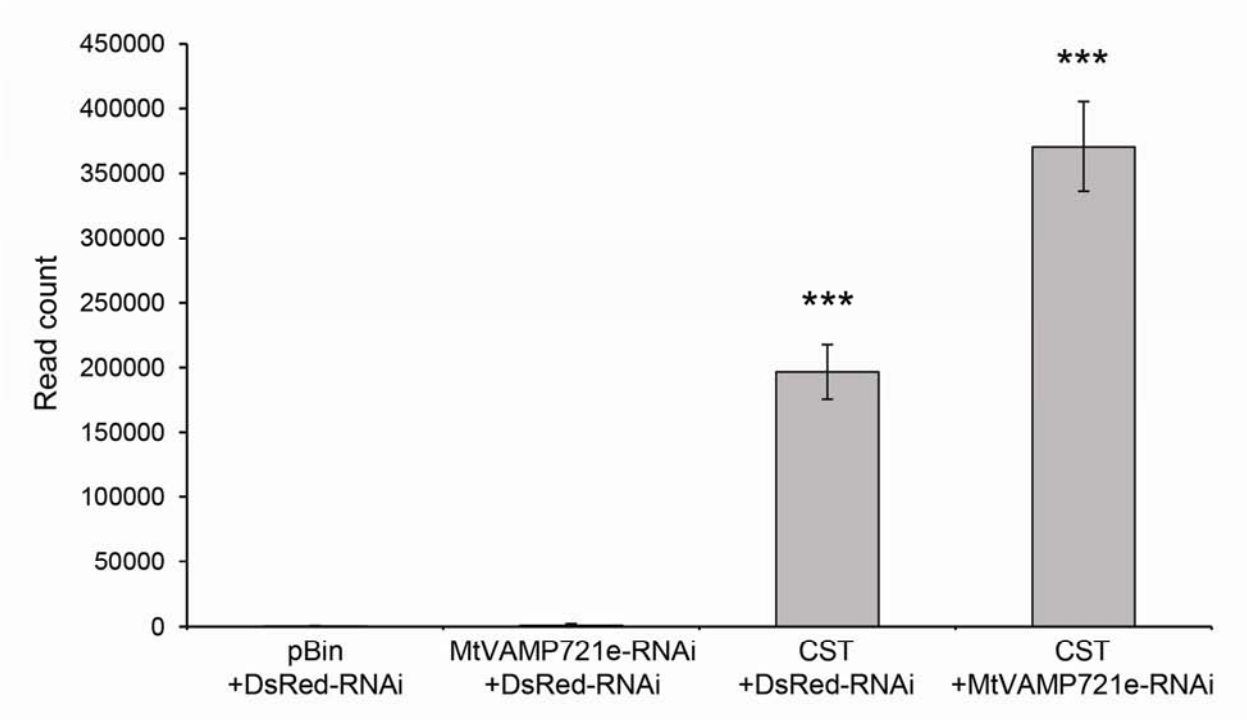

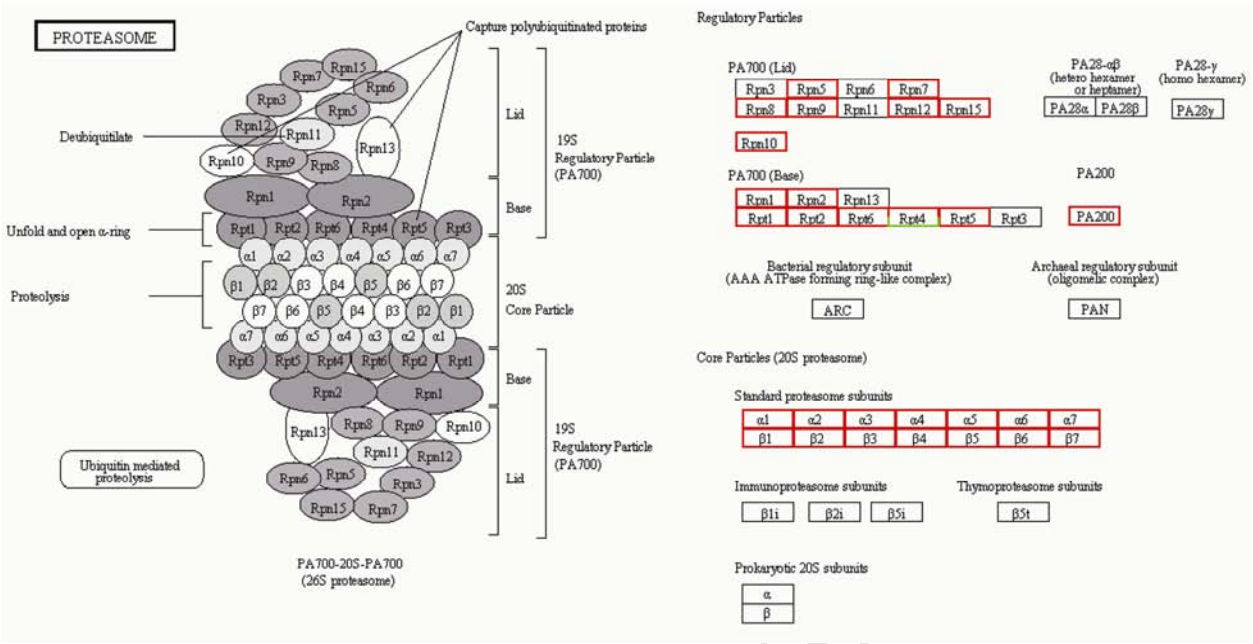

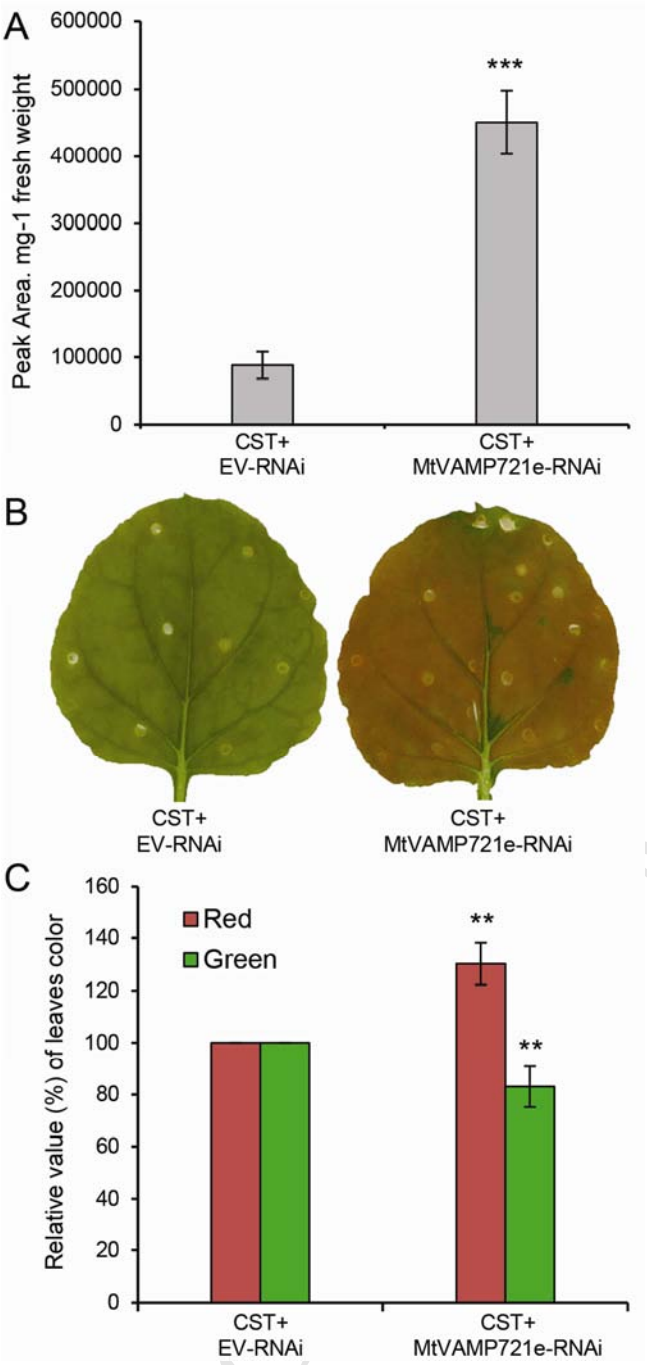

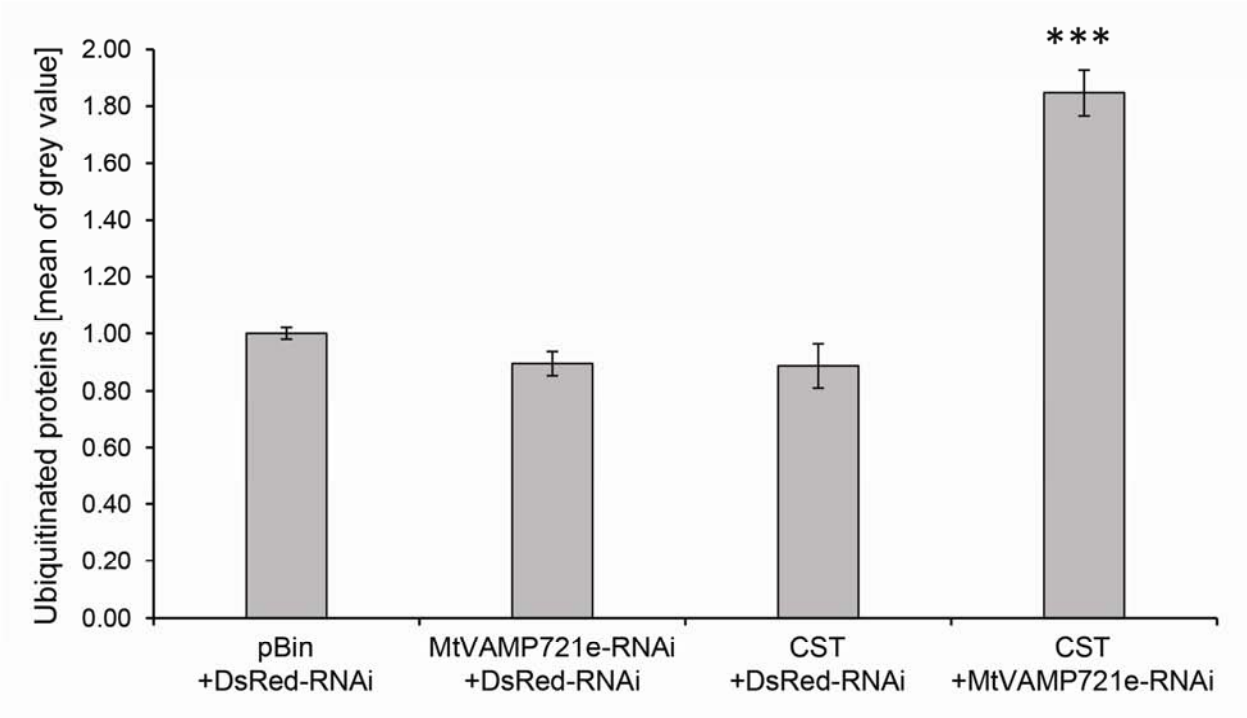

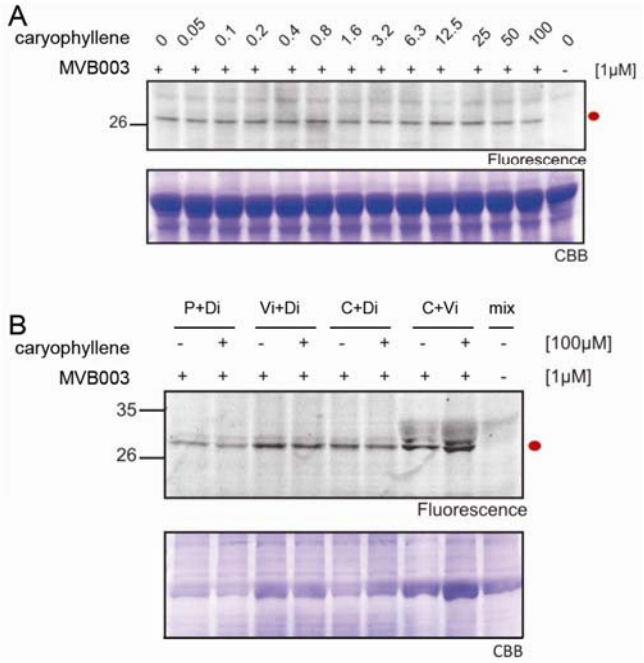

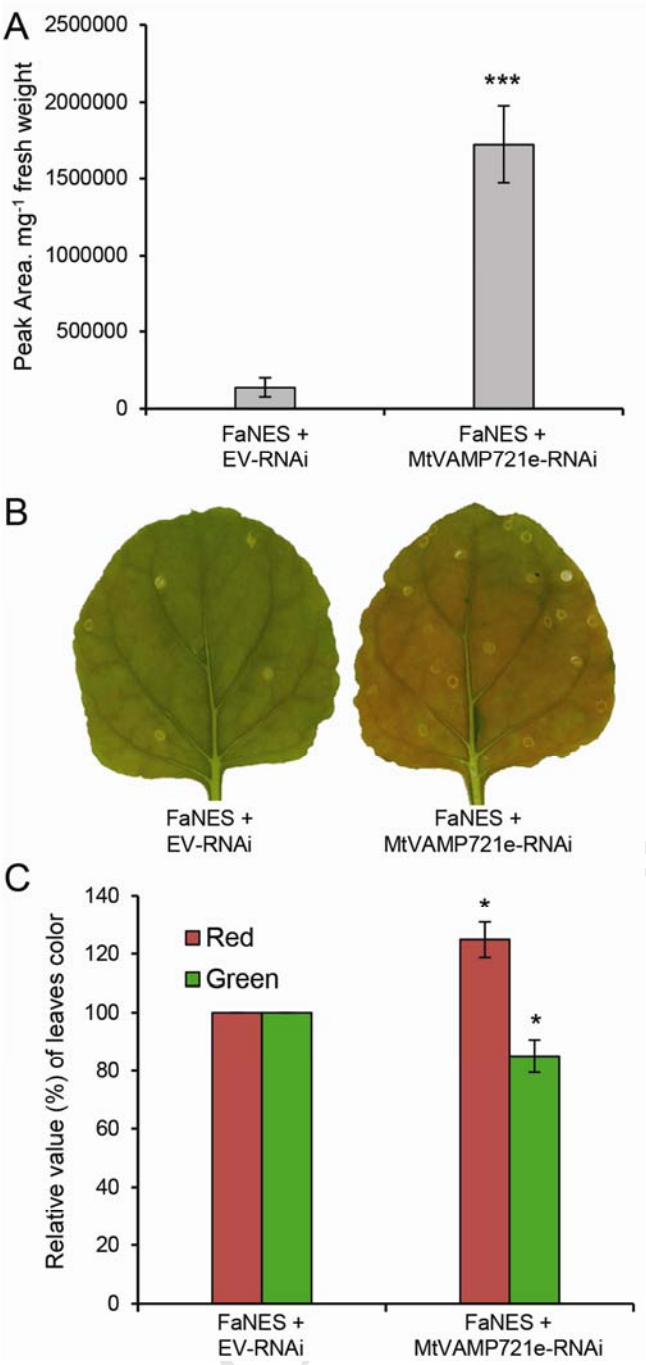
A
Peak Area. mg-1 fresh weight
2500000
2000000
1500000
1000000
500000
0
***
FaNES + EV-RNAi
FaNES + MtVAMP721e-RNAi
B
FaNES + EV-RNAi
FaNES + MtVAMP721e-RNAi
C
Relative value (%) of leaves color
140
120
100
80
60
40
20
0
Red
Green
*
*
FaNES + EV-RNAi
FaNES + MtVAMP721e-RNAi